Research Article | Vol. 12, No. 10 / 1 Oct 2021 / Biomedical Optics Express 6237
Biomedical Optics EXPRESS

Light-sheet fluorescence microscopy for the *in vivo* study of microtubule dynamics in the zebrafish embryo

MATTEO BERNARDELLO,[1,2] MARIA MARSAL,[1,2] EMILIO J. GUALDA,[1,2] AND PABLO LOZA-ALVAREZ[1,*]

[1]*ICFO-Institut de Ciencies Fotoniques, The Barcelona Institute of Science and Technology, Castelldefels, 08860, Spain*
[2]*equal contribution*
[*]*pablo.loza@icfo.eu*

Abstract: During its first hours of development, the zebrafish embryo presents a large microtubule array in the yolk region, essential for its development. Despite of its size and dynamic behavior, this network has been studied only in limited field of views or in fixed samples. We designed and implemented different strategies in Light Sheet Fluorescence microscopy for imaging the entire yolk microtubule (MT) network *in vivo*. These have allowed us to develop a novel image analysis from which we clearly observe a cyclical re-arrangement of the entire MT network in synchrony with blastoderm mitotic waves. These dynamics also affect a previously unreported microtubule array deep within the yolk, here described. These findings provide a new vision of the zebrafish yolk microtubules arrangement, and offers novel insights in the interaction between mitotic events and microtubules reorganization.

1. Introduction

During the first hours of embryonic development, microtubules (MT) can be found ubiquitously along the zebrafish (*Danio rerio*) embryo. In the blastoderm, siting at the animal pole, MT are mainly responsible for cell divisions and are highly condensed during mitosis in the mitotic spindles. In the yolk cell, an initially a-nuclear lipid sphere of roughly 700 µm in diameter [1], MTs are also present and account for transport of molecules essential for early development [2–5]. The current view for the MTs organization in the yolk cell describes a network of parallel MTs that emerge from the marginal blastomeres, extend towards the vegetal pole and are located at the superficial region of the yolk cell, in the Yolk Cytoplasmic Layer (YCL) [3,6–9]. Reaching the 512-cell stage, a syncytium forms in the yolk, called Yolk Syncytial Layer (YSL) [1], containing the Yolk Syncytial Nuclei (YSN) [8], which derive from the collapse of the marginal cells and the release of their content into the yolk mass. YCL MTs are believed to be associated with the most vegetally located external YSN (eYSN) once the YSL has been formed. These parallel MT arrays have been studied mainly for their role in the mechanism of epiboly, and have been proved to be necessary for the correct migration of the eYSN toward the vegetal pole [7], through associated motor proteins [9]. Besides that, the presence of a MTs mesh in the internal YSL (iYSL) between the internal YSN (iYSN) and eYSN, has also been described [6–8]. However, little is known about the organization and changes that the yolk MT network presents at cleavage and blastula stages. In this temporal window it is assumed that the parallel arrays are associated to the marginal blastomeres [7], but no extensive data is available to describe how this network is maintained and eventually re-organized over a long period of time until the initiation of epiboly. Most studies are conducted by fixing embryos at various time points, hiding the potential transient dynamics. Live-imaging has also been performed using confocal microscopy [3,7,10,11]. This method however, provides limited field of views (FoV), has poor penetration capabilities and

#438402 https://doi.org/10.1364/BOE.438402
Journal © 2021 Received 23 Jul 2021; revised 21 Aug 2021; accepted 24 Aug 2021; published 13 Sep 2021

Biomedical Optics EXPRESS

has the potential to induce unwanted phototoxic effects. Therefore, these approaches (use of fixed embryos, visualization of small field of views, or use of confocal microscopy) are far from providing an accurate and complete description of the dynamic nature of the MT network over the full yolk sphere. The study of this MT network in its full complexity would provide the basis for the description of its role before the initiation of epiboly, and it would offer an *in vivo* model for the study of MT dynamics and its organization in a scale that largely encompasses the size of ordinary cells.

In many biological systems signals need to travel across the cellular environment. Although this could be achieved at small scales through molecule diffusion, the mechanism would not be efficient at large scales [12], i.e. where signals need to induce spatio-temporal coordination over distances of hundreds of micrometers. In such large-scale environments many examples of wave-like patterns can be found. Wave-like patterns consist in the cascade of a particular event that appears to cross the system. The events are synchronized between them in such a way that it is possible to visualize a travelling wavefront. Examples of wave-like patterns include the bulk actin wave in zebrafish oocytes [13], calcium waves [14,15], and mitotic waves in zebrafish [1,16,17], in Xenopus embryos [18], and in Xenopus egg extracts [19].

Light Sheet Fluorescence Microscopy (LSFM) [20] provides an efficient way for *in vivo* imaging of large samples and at high resolutions [21]. In fact, in zebrafish development, LSFM has been extensively and successfully used to observe nuclei movements and to describe cells' fate in the entire embryo or of specific germ layers [16,22–24]. Here instead, we designed and implemented our custom-made LSFM setups (see Methods section) to observe the dynamical changes in the structure of the zebrafish external YCL MT network (eMTN). Our two setups, based respectively on agarose [20] and fluidic [25] sample mounting methods, enable to image living zebrafish embryos within their native chorion. This possibility is of exceptional importance for a correct live imaging session, as it avoids the mechanical constrictions that conventional agarose medium, such as the ones used in confocal microscopy, could exert on the sample development. Moreover, the sample orientation can be easily adjusted thanks to the motorized rotational stage. This imaging flexibility is not possible in conventional confocal microscopes, and it provides a clear advantage for the study over a prolonged time of living organisms. In addition, the temperature at which the embryos develop can be controlled and maintained constant for the whole experiment.

We focused on cleavage and blastula temporal windows, interested to gain insight into the MT network dynamic nature over the entire yolk. Along the present work, we will show and characterize a particular feature, firstly indicated in [11] in a limited spatio-temporal window, but to our knowledge not yet described in its full dimensions: Microtubule Organizational Waves (MOW) that cross the yolk cell. Here we present the MOW as a new wave-like pattern. Besides its visualization, we also correlate it with other macro-events happening in the embryo, such as a constriction and relaxation of the blastoderm margin and the cells' division cycles. In addition, we also provide a set of dedicated tools for the image quantification of this phenomenon, considering the spherical shape of the embryo. Moreover, we give evidence of the presence of another set of MTs present deep into the yolk, the internal MT network (iMTN), and show how it is affected by the MOWs' passage. Previous work based on embryos' fixation and immunostaining could not conclude on the eventual existence of the iMTN [7] and only now, thanks to the penetration depth provided by *in vivo* LSFM, this new MT network can be rigorously investigated.

Taken together, our results permit to provide a more complete vision of the MT networks populating the zebrafish yolk cell, both in their morphology and their dynamics. In turn, the zebrafish yolk MT networks emerges as an *in vivo* model to test different hypotheses on microtubule-based nucleation and on the interaction between mitotic waves, centrosomes, and MT branches [26].

Biomedical Optics EXPRESS

Our methodology, based on LSFM and a novel image analysis procedure, has the potential to further investigate new and already approached problems in various temporal windows. Examples might extend from a complete description of large scale transport of molecules and organelles to an all-embryo global view on the MT-based epiboly movements. Moreover, these can be quantitatively assessed in various early zebrafish development mutants showing alterations in MT organization.

2. Methods

2.1. LSFM setups

For this work, we designed and implemented two different LSFM setups, which differ in the sample mounting procedure (conventional agarose-based and fluidics). These allowed for prolonged imaging sessions in large Field of Views (FoV). These setups have been optimized to image the MT reporter transgenic line TG(XlEef1a1:dclk2-GFP) [10]. In both setups, the excitation light is provided by a laser at 488 nm. Being the zebrafish embryo a large organism of roughly 700 µm in diameter, two illumination air objectives (Nikon 4x, 0.13NA, placed one on each side of the embryo) were used in an alternated excitation scheme to sequentially irradiate the sample from both sides and improve image quality, while one detection water objective (either Nikon 10x, 0.3NA or Olympus 20x, 0.5NA) was used to collect the emitted fluorescence photons.

In order to be mounted in the first LSFM, embryos, without removing the chorion, were embedded into a 1.5% low melting point agarose (lmpa). The lmpa cylinder is extruded from a glass capillary hanging from the imaging chamber's top, and being connected to a translational xyz stage, as described in [27] (Fig. 1(A)). In addition, rotation of the sample with respect to the vertical axis is also implemented through a stepper motor for the proper orientation of the specimen. The imaging chamber integrates at its bottom a heating block to maintain constant (through a Proportional-Integrative-Derivative (PID) algorithm) the temperature of the imaging medium. The imaging medium temperature is also monitored and logged to the controlling computer through a temperature sensor. The illumination of the embryo's volume is obtained by the sample's motorized translation across the vertical light sheet(s) generated by two cylindrical lenses (ACY254-150-A, f=150 mm, Thorlabs) followed by the two illumination objectives (as in the Selective Plane Illumination Microscopy – SPIM - configuration [20]). In each of the illumination arms, a shutter is present to alternatively block or allow the passage of the light, and to obtain the sequential illumination of both sides of the specimen (Fig. 1(B)). Each shutter has been implemented via a 3D printed bar inserted in the light path and moved by a servo motor, which is controlled by the custom-made microscope software.

In the second LSF microscope, the embryo was loaded into a fluidic circuit composed of a 1 mm FEP tube [25,27] (Fig. 1(C)). The FEP tube crosses at 45° the imaging chamber, and a dedicated syringe pump permits to transport the sample to the FoV of the vertically positioned detection objective. A galvanometric scanning mirror (placed in a conjugated plane with the two illumination objectives), generates the horizontal light sheets (as in the Digital Scanned Laser Light Sheet Fluorescence Microscopy - DSLM - configuration [16]), and the volume is scanned by the motorized movement of the entire chamber containing the FEP circuit. As in the previous system, shutters are used to select which side of the embryo to illuminate, allowing the alternate excitation (Fig. 1(D)).

In both setups, 3D z-stacks were acquired by sample scanning with z-step ranging from 1 to 2 µm, and typically 60 to 90 seconds between two consecutive volume acquisitions. The collected fluorescence was projected through tube lenses (AC254-200-A-ML, f=200 mm, Thorlabs) onto the chip of a sCMOS camera (Hamamatsu Orca Flash4.0). Imaging sessions started during cleavage and blastula stages of the embryos, typically between 32 to 128 cell stages. The double illumination scheme produces for each embryo two set of images stacks, which maximum intensity projections and 3D stacks images were fused together either using the FIJI [28] plugin

Biomedical Optics EXPRESS

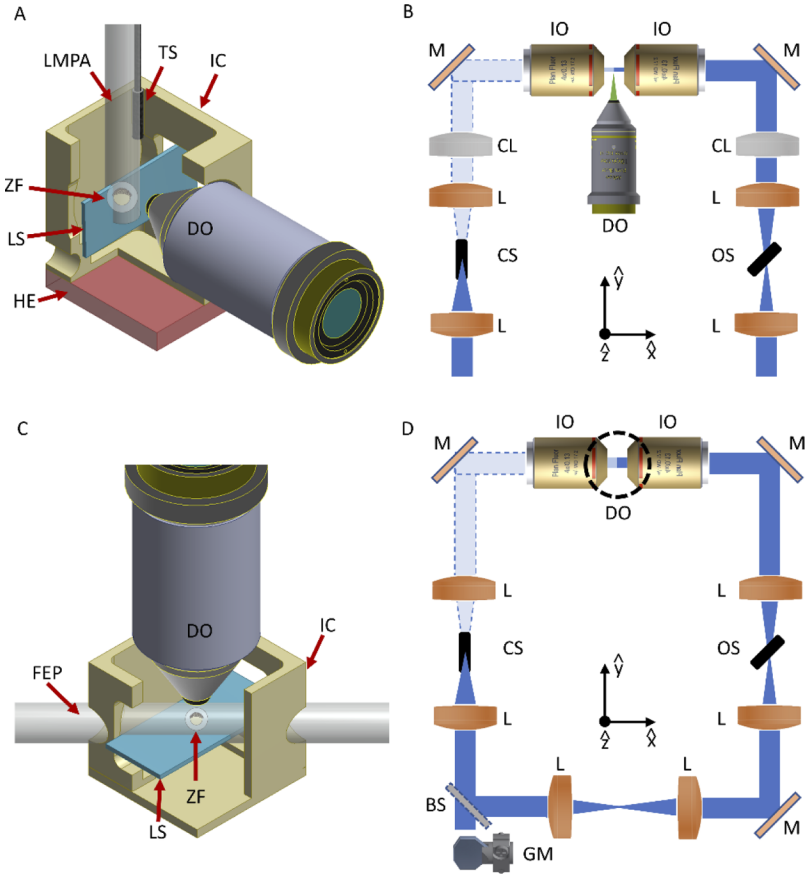

Fig. 1. Schematic of the LSFM mounting and scanning methods used. (A) The zebrafish embryo (ZF), within its chorion, is embedded inside a lmpa cylinder hanging from the top of the imaging chamber (IC) and connected to a translation-rotational stage, to enable the scan through the vertical light-sheet (LS). The emitted photons are collected by the detection objective (DO). A heating element (HE) is integrated below the chamber, while a temperature sensor (TS) is immersed in the imaging medium to monitor the temperature for the whole experiment. (B) Schematic of the illumination optical path for the first LSFM setup. Each of the two illumination arms contains two lenses (L) and a cylindrical lens (CL) for the LS formation. After reflection on a mirror (M), the illumination objective (IO) generates the vertical LS in the sample plane. The illumination paths also contain two shutters (CS = closed shutter, OS = open shutter), that are employed to block the light from one of the two arms, generating the alternate illumination scheme. (C) A FEP tube crosses at 45° the imaging chamber, creating a fluidic circuit through which the embryo is loaded and then positioned in the FoV of the detection objective. Once here, the entire chamber (and the attached FEP tube) is displaced vertically to scan the sample across the horizontal LS. The imaging chamber models are here sectioned to ease visualization of the interior part. (D) Schematic of the illumination optical path for the second LSFM setup. A galvanometric mirror (GM) generates the LS that through a beam-splitter (BS) is sent to each illumination objective, to create the horizontal LS at the sample plane. The dotted circumference denotes the position of the vertical detection objective. Shutters are again used to implement the double alternate excitation scheme. $\hat{x}$ and $\hat{y}$ denote the horizontal plane, while $\hat{z}$ denotes the vertical axis.

Biomedical Optics EXPRESS

"Pairwise Stitching" [29] or a custom-made FIJI macro. Image analysis was performed through dedicated workflows (see Results sections and Supplement 1 for further details) on the produced data without image intensity treatment. Only the images of one embryo (showed in Fig. 2(A), Fig. 3, and Visualization 2) were treated with the FIJI plugin "Bleach Correction" through an exponential fit to account for photobleaching through time before the analysis. See also the Supplement 1 for further details.

3. Results

3.1. LSFM permits the visualization of the MTs re-arrangement in the whole embryo

Thanks to the big FoV of our custom-build LSFM system (maximum 1330 µm × 1330 µm), we have been able to follow the development of whole zebrafish embryos at high spatial (ranging from 0.60 µm to 1.45 µm) and time resolution (ranging from 0.3 to 1 volumes/minute). In order to visualize MT dynamics, we used the MT reporter transgenic line TG(XlEef1a1:dclk2-GFP) [10] (noted as dclk2-GFP). In addition, as MT spindles are a key component during mitosis, the dclk2-GFP line also provides useful information about their spatial (e.g, orientation of the divisions) and temporal behavior (e.g, synchronization between them and other events).

From our images it is particularly evident how the concentration of microtubules changes during the division cycle of both blastomeres and YSNs. This is because during metaphase the spindles produce a higher fluorescence signal that then rapidly decreases until interphase, providing a measure of the cell cycle timing. By following the mean intensity profile of the entire blastoderm over time (Fig. 2(A)), it was possible to account for the different cell cycles stages. In fact, this mean intensity value follows alternatively peaks and valleys, which correspond to the meta- and inter- phases of the cell cycle respectively (Fig. 2(B)). This analysis provides a means of staging the embryo under observation, which can be later used for additional analysis. The correspondence between intensity peaks and valleys with the mitosis events remains valid also when smaller regions are analyzed. Therefore, it allows us to follow up locally the timing of the division cycles of single cells or YSN.

The dclk2-GFP line provides not only the visualization of the MT spindles during the division cycles of the blastomeres and YSN, but also of the MT network in the yolk. Through our custom-made LSFM setups, we mesoscopically analyzed the *in vivo* dynamics of the eMTN during cleavage, blastula, and gastrula stages over the entire yolk cell. As the eMTN is located in the YCL, we can visualize it through the maximum intensity projection of the acquired 3D stacks (Fig. 2(A)).

We observed that the MT network periodically and progressively undergoes a reorganization process over time (Visualization 1), forming what we called Microtubule Organizational Waves (MOWs). These subsequent wave-like patterns consist of variations in MTs density, either due to cyclical polymerization and de-polymerization [11] or bundling and unbundling events. The measure of the mean intensity over a determined region of interest (ROI) correlates with a measure of the density of the microtubules present in the same region (Fig. 2(C)). Therefore, the drop of the mean intensity, from a higher value (dense network and low bundling levels of microtubules) to a lower value (sparser network), correlates with the passage of the MOW wavefront in that region. Several MOWs can be visualized sequentially in a given ROI between cleavage and blastula stages, before the initiation of epiboly. They appear to originate from the blastoderm margin and advance, in a belt-like fashion, towards the vegetal pole, where they concentrically close (Fig. 2(D)-(F)). A closer look reveals that before the passage of the MOW the MT network appears to be diffused and disorganized, without a clear and precise orientation (Fig. 2(G)). At the passage of the MOW, the involved microtubules appear to be re-organized in well-defined and thicker bundles (Fig. 2(H)). Shortly after, they become again diffused (Fig. 2(I)) and the following MOW will repeat the bundling process.

Biomedical Optics EXPRESS

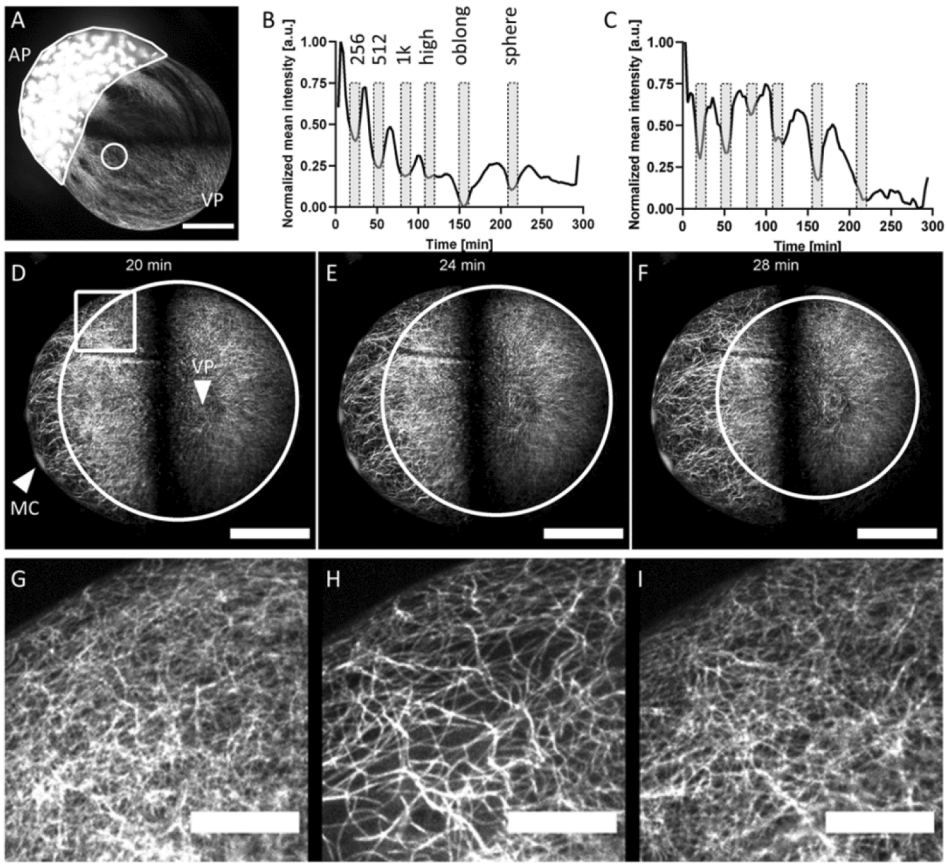

Fig. 2. LSFM permits to see the microtubule re-arrangement in the whole embryo. (A) dclk2-GFP embryo during synchronous mitosis events of the blastomeres. Lateral view, AP = animal pole, VP = vegetal pole, scale bar 200 µm. (B) Normalized mean intensity profile over time of the blastoderm region as highlighted in (A). The overlaid bars indicate the subsequent developmental stages of the embryo, from 256-cell to sphere stage. (C) The obtained graph for the normalized mean intensity over time on the yolk surface (circular ROI in (A)). Overlaid bars highlight drops of intensity corresponding to MOW passages. (D-F) Three frames (maximum intensity projection) from time-lapse LSFM imaging of the same embryo. The white circumferences indicate the wavefront of the same MOW that is advancing over the eMTN of a dclk2-GFP embryo at cleavage stage, vegetal view. During time, the wavefront travels toward the vegetal pole of the embryo (the travelling is indicated by the reducing size of the overlapped circumference). See also Visualization 1. MC = marginal cell, scale bar 200 µm. Central black region is due to the LS bending caused by the curvature of the sample. (G-I) Zoom in at the square region highlighted in (D), visualizing the eMTN (G) before (diffuse network), (H) during (sparser MTs), and (I) shortly after (re-diffused network) the MOW passage. Scalebars 50 µm.

Biomedical Optics EXPRESS

3.2. Temporal concurrence of mitosis and MOWs

It is accepted that the microtubules at the YCL emerge from microtubule organizing centers (MTOCs) associated with the marginal cells (or eYSN, when formed) [6,7].

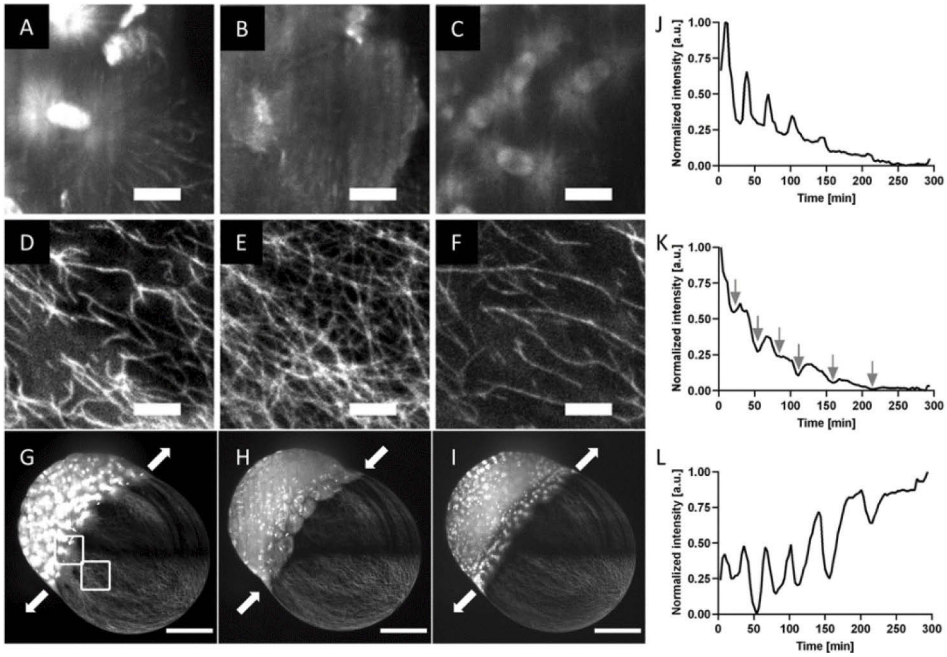

Fig. 3. Temporal concurrence of mitosis and MOWs. (A-C) Visualization of blastomere/eYSN cycle phases (relative ROI indicated in panel (G)) through microtubules' labelling: (A) metaphase, (B) interphase, (C) metaphase (at minutes 9, 24, 102). Scale bars 25 µm. (D-F) Visualization of MOWs passages in the subsequent yolk region (relative ROI indicated in panel (G)). The MT network is (D) highly oriented and sparse, then (E) re-diffuses, and again (F) sparse (at minutes 15, 27, 108). Scale bars 25 µm. (G-H) The same dclk2-GFP embryo from a lateral view at three different timepoints (at minutes 9, 24, 102), scale bars 200 µm. Animal pole at top left, vegetal pole at bottom right. Arrows indicate expansion (pointing outward in A and C) and contraction (pointing inward in B) of the blastoderm margin. (J) Normalized mean intensity graph visualizing blastomeres/YSNs cycles (metaphases are peaks, interphases are valleys, graph obtained from the local analysis). (K) Normalized mean intensity graph visualizing the periodic MOWs passage (arrows) over the yolk region (graph obtained from the local analysis). (L) The periodic blastoderm contractions (valleys) and expansions (peaks). Blastoderm margin expansion and nuclei metaphase appear to be synchronized, MOW passage follows after few minutes. See Supplement 1 for details on how the graphs were retrieved. See also Visualization 2.

From this work, it also appears that the dividing blastomeres potentially also induce the division of the connected MT branch, giving rise to two sub-branches (see Supplement 1 Fig. S1). As previously described, MOWs pass across the yolk from the blastoderm margin to the vegetal pole (see also Visualization 2). We therefore examined the temporal concomitance between the MOWs initiation and the division of the blastomeres/eYSN generating the microtubule branch. Interestingly, the MOWs appear to be synchronized with the division cycle of the blastomeres/eYSN (Fig. 3(A)-(C)). Moreover, the re-organizational process of the microtubules in the yolk cell (Fig. 3(D)-(F)) appears to be also synchronized with cyclic embryo macro-scale

Biomedical Optics EXPRESS

shape changes, such as constriction at the blastoderm margin, followed by expansion periods (Fig. 3(G)-(I)).

In order to demonstrate the temporal concomitance between MOWs initiation and the division cycle of the blastoderm cells we recorded, for all the time points, the mean intensity of the closest to the YSL part of a yolk's microtubule branch and the mean intensity of the cell (or eYSN) that appear to generate that branch (through the FIJI plugin "Manual Tracking with Trackmate" [30], see also "local analysis" section in Supplement 1). For cells and eYSN analysis, a peak in the mean intensity corresponds to a mitotic event (Fig. 3(J)). Over the microtubule branch, a drop in the mean intensity corresponds to a MOW passage (Fig. 3 K). The periodic constriction and expansion of the blastoderm margin was also detected (Fig. 3(L)). The analysis confirms a temporal correlation of these three events, which would suggest that they are closely related. In particular, while the blastoderm margin contractions are temporally concomitant with the blastomeres' divisions, the MOW initiations follow with a slightly delayed timing.

3.3. MOWs depend on the cell/eYSN divisions

One of the major events that occurs prior to gastrulation is the fact that the eYSNs become post-mitotic, coinciding with the beginning of epiboly [31]. Given the low photobleaching and phototoxicity properties of LSFM setups, we can image the development of our embryos throughout all the embryonic developmental stages, from cleavage to beyond epiboly (see Visualization 3). This allows us to examine when the last MOW takes place, in order to correlate the origin of the MOWs with the divisions of blastomeres or eYSN. From visual inspections, no MOW is emerging during gastrulation. To further investigate it, we detected the time points of last divisions of the eYSNs (see also Supplement 1) and compared them with the last MOW's initiation timing. Nuclei are visible as non-fluorescence spots over a bright (microtubules) background (Fig. 4(A)), except when the division takes place, i.e. when the mitotic spindles increase the fluorescent signal (Fig. 4(B)). MT density variations defining the MOW initiation (Fig. 4(C)-(D)) are retrieved, and the comparison of the obtained graphs (Fig. 4(E)-(F)) supported our hypothesis (i.e. the last MOW's initiation is temporally correlated with the last division of eYSNs) in five out of six examined embryos.

In order to gain further evidences of the dependence of the MOWs initiation on the blastomeres/eYSN divisions, we sought to interfere with the periodicities of their division's cycles. A simple but effective method is given by the sensitivity of the embryo to the temperature. It is well established that the division timing of the blastoderm is influenced by the temperature of the medium in which the embryo is immersed: higher temperatures will accelerate the processes, while lower temperatures will consistently delay the division cycles [1]. Through our LSFM imaging chamber, the temperature of the imaging medium in which the embryos are immersed can be controlled, and permitted to follow embryos' development at three different temperatures: 22, 26.5, and 31 degrees Celsius. On the retrieved images, we tracked the YSN and the relative branch mean intensities over time to detect the time points in which (1) the mitosis events and (2) the MOW initiation occurs. Finally, periodicities, defined as the time elapsed between one event and its immediately precedent occurrence, were calculated for both MOWs and mitosis. Figure 4(H) shows how temperature affects, as expected, the division periodicity of the blastomeres or eYSN's mitosis (33.79 ± 12.79 min at 22 degrees, N=21; 22.77 ± 5.32 min at 26.5 degrees, N=11; 19.38 ± 7.05 min at 31 degrees, N=12; means ± standard deviations). It can also be observed how the periodicities of the MOW's initiation change according (35.56 ± 11.32 min at 22 degrees, N=17; 22.17 ± 5.94 min at 26.5 degrees, N=12; 18.53 ± 6.25 min at 31 degrees, N=17; means ± standard deviations). Importantly, no statistically significant difference was observed between mitosis' periodicities and MOWs' initiation periodicities relative to the same experimental condition, which confirms our hypothesis that MOWs' initiations closely follow mitosis events in their variation due to temperature.

Biomedical Optics EXPRESS

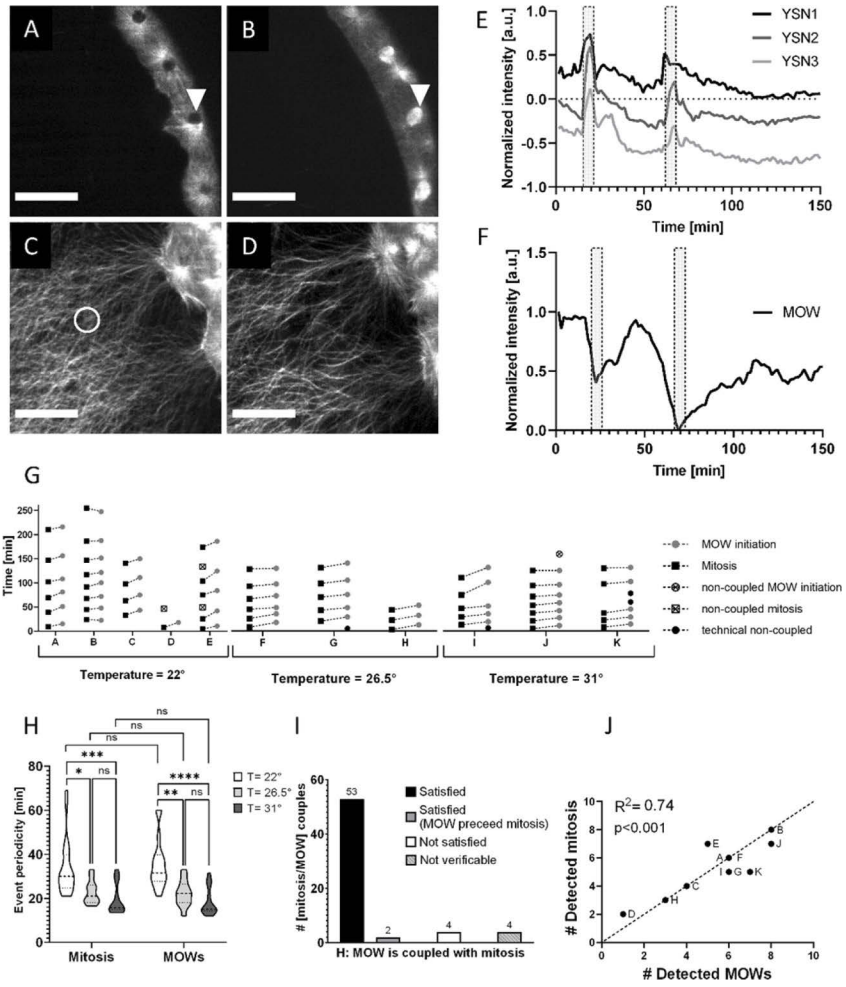

Fig. 4. MOWs depend on the cell/eYSN divisions. (A-B) Internal slices from the 3D stack showing the YSN (white arrow) before (A) and during (B) a mitotic event. (C-D) Maximum intensity projection for the same area in (A-B), showing the MT network emerging from the YSN, before (denser network, C) and after (sparser network, D) the YSN mitotic event. Scale bars 50 µm. (E) Normalized mean intensity profiles of three YSN tracked through the 3D stack over time, recording their last two divisions (overlaid bars). For better visualization, an incremental offset is applied to avoid graphs' overlapping. (F) Normalized mean intensity profile from a 19 µm ROI (white circumference in (C)) over the MT branch from the maximum intensity projection over time. The retrieved graph records the last two MOWs' initiations (overlaid bars), corresponding to the YSN divisions in (E). (G) Time points at which mitosis (squares) and MOWs' initiations (circles) happens, for embryos at different temperatures. Each letter identifies one embryo. (H) Violin plots resuming the effect of experimental temperature on periodicities of mitosis (left part) and MOWs' initiations (right part). p-values: ns = $p>0.05$, *= $p<0.05$, **= $p<0.01$, ***= $p<0.001$, ****= $p<0.0001$. (I) Overview on the 63 analysed [mitosis/MOW initiation] coupled events and their outcome to the hypothesis "MOW initiation coupled with mitosis". (J) Correlation graph between the number of detected MOW initiation and of detected cell/YSN divisions from each embryo (letters). Dotted line represents identity line. See also Supplement 1 Fig. S2.

Biomedical Optics EXPRESS

Besides demonstrating that the interference with the mitosis cycle also affects MOW's initiations timing, from our experiment we can also infer that there is a one-to-one relationship between every division (cell or eYSN) and MOW's initiation. This correspondence is independent of stage and temperature. This is easily visualized by plotting the exact timing for each event, highlighting how the correspondence between each mitosis and MOW initiation is consistent throughout the analyzed embryos (Fig. 4(G)). In our analysis, this hypothesis was confirmed in 55 cases out of 63 (Fig. 4(I)). The remaining 8 hypothetical [mitosis-MOW] couples were lacking either the mitosis event or the MOW initiation event. This could be explained due to the presence of biological outliers (4 cases) or due to technical imaging issues, in which the cells were out of the FoV or their hypothetical division happened before the start of the imaging, and therefore the hypothesis outcome could not be verified (4 cases). The association between the two events can also be visualized through the graph depicted in Fig. 4(J), showing a strong positive correlation (Pearson correlation coefficient $r=0.86$, $R^2=0.74$, $p<0.001$) between the detected number of MOW initiation and detected mitosis, for the different embryos.

3.4. MOWs' global visualization and analysis

Having observed the MOWs' propagation from the blastoderm margin towards the vegetal pole, we developed a dedicated image analysis tool to characterize it (see "global analysis" section in Supplement 1). This tool for global MOW analysis models the yolk as a sphere and it defines, over the spherical surface, meridians (the set of points having the same azimuth angle) and parallels (the set of points having the same elevation angle), as shown in Fig. 5(A). By back-projecting the calculated coordinates onto the 2D image, the mean intensity over time of a 50 µm ROI travelling over the meridians (Fig. 5(B)) can be measured. From these values, and considering its spherical shape, a kymograph of the evolution of the microtubule dynamics over the whole imaged yolk's surface along specific meridians is produced from blastoderm margin to the vegetal pole (Fig. 5(C)). The connections of the intensity valleys between subsequent points of the same meridian identify the presence of various MOWs, and prove their propagation over the yolk's surface. In this way, the speed of the different waves can also be measured in degree/min along each meridian, i.e, for different MT branches. Applying this tool to embryos developing at different temperatures, we have measured the MOWs' propagation speeds over the yolk sphere to vary from 2.45 ± 0.59 degrees/min to 4.70 ± 1.50 degree/min which correspond to linear speed ranging from 14.42 ± 3.47 µm/min to 26.27 ± 8.38 µm/min (means ± standard deviations, see also Supplement 1 for calculation details).

MOWs however, are not the only wave-like events happening in the embryo. In the first stages of development the cells forming the blastoderm divide synchronously but subsequently, as the embryo develops, the cells' divisions lose this synchronicity becoming "metasynchronous". Cells closer to the animal pole divide first and marginal cells afterwards, producing a wave-like pattern [1,16,17]. Modelling the blastoderm as a hemisphere in the same way, the above-mentioned analysis can be repeated highlighting the propagation of the mitotic wave along the meridians defined over the blastoderm (Fig. 5(D)). This analysis also shows that MOWs' initiations are slightly delayed with respect to the blastomeres/eYSN divisions (Fig. 5(E)), which would be in agreement with our hypothesis that the divisions could be the trigger of the MOW phenomena.

Through the same tool, the mean intensity kymograph can also be constructed also along the parallels of both the yolk and blastoderm hemispheres (Fig. 5(F)), which provides a way to visualize MOWs' and mitotic waves' wavefronts and to analyze their symmetry with respect to the animal-vegetal (AV) axis (Fig. 5(G)-(H)).

3.5. A novel MT network is present deep inside the yolk

LSFM greatly improves the penetration depth respect to confocal microscopy, providing a unique opportunity to study the morphology and dynamics of the inner part of the zebrafish yolk. Despite

Biomedical Optics EXPRESS

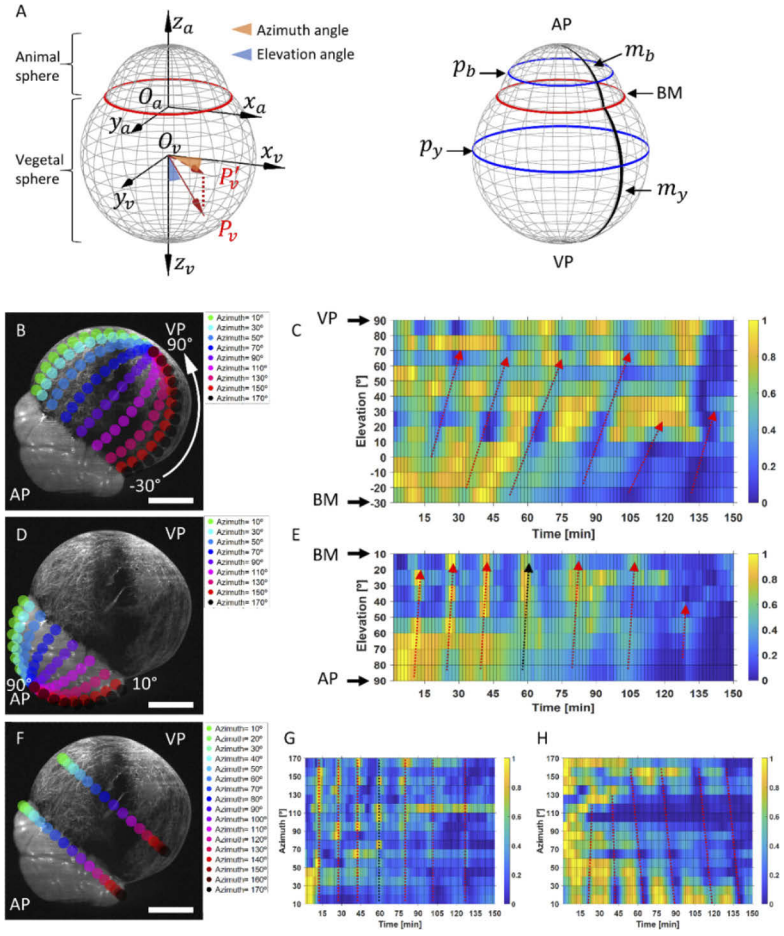

Fig. 5. MOWs' global visualization and analysis. (A) Left panel: representation of the coordinates system and spherical coordinate convention of the double-hemisphere 3D model for the zebrafish embryo. Pv is a general point over the spherical yolk surface, and P'v its projection on the xy plane. Right panel: exemplification of meridians (black) and parallels (blue) on the blastoderm (mb, pb) and yolk sphere (my, py). In both panels, the red circumference represents the blastoderm margin. AP = animal pole, VP = vegetal pole, BM = blastoderm margin. (B) Maximum intensity projection of LSFM imaging of a dclk2-GFP embryo, lateral view, and some of the paths followed to adapt the analysis to the spherical yolk shape. Scale bar 200 µm. (C) Normalized mean intensity kymograph relative to a single meridian of the yolk sphere, over time. Intensity drops (red arrows) reveal MOWs' passage from BM to VP. Speed calculation is performed through slope measurement (elevation angle/time). (D) Some of the paths followed to perform the analysis over the blastoderm hemisphere. Scale bar 200 µm. (E) Normalized mean intensity kymograph relative to a single meridian of the blastoderm hemisphere, over time. Intensity peaks (arrows) reveal the mitotic wave passage from AP to BM. From comparison of (C) and (E) is shown how MOWs follow in time the mitosis but also, in this particular embryo, the presence of an outlier as one mitosis (black arrow in E) is not followed by any MOW. (F) Over the maximum intensity projection of the same embryo (scale bar 200 µm), the analysis along parallels is performed. This produces the normalized mean intensity kymographs relative to blastoderm (G) and yolk (H), showing the wavefronts (dotted lines) of the mitotic waves (G, black dotted line indicates the outlier) and MOWs (H).

Biomedical Optics EXPRESS

the current view, which refers only to the MTs mesh around the iYSN and to the MTs branches in the external YCL (the eMTN) [3,6–8], we found that an intricate network of MTs is also present deep inside the yolk. To our knowledge, this internal MTs network (iMTN) was not previously reported. With LSFM we proceed then to describe in detail its morphology and its dynamics, correlating it with the MOWs passages and the eYSN mitosis.

The iMTN appears to be uniformly present in the whole yolk and its presence was consistently observed in all the LSFM examined embryos. From a 3D vegetal view of a blastula embryo, we digitally removed the YCL and the related MTs network to visualize how this network spans the yolk until at least a depth of 350 µm from the vegetal pole (Fig. 6(A)). As visualized in Fig. 6(B) as maximum intensity projection of a 40 µm range, the internal MT network appears to be uniformly distributed also in the lateral direction. We found that several MTs form circular-like pattern, most probably surrounding the lipid granules, which are known to fill the yolk [1,17]. Additionally, several MTs are connected to the MT network present in the YCL and between them (Fig. 6(C)). More intriguingly, clear connections were found between the eYSN associated centrosomes with microtubules directed towards the interior part of the yolk, which we believe to be part of the iMTN (Fig. 6(E)-(I), Visualization 4, and Visualization 5). To verify the presence of the iMTN on wild-type (WT) embryos, we fixed and immunostained them with an anti-β-tubulin antibody [32,33] (see Supplement 1), and imaged them with the same LSFM setups. Although the fixation step in the immunostaining protocol enhances the autofluorescence of the yolk, specific tubulin signal is detected in its internal part, which would come from the microtubules associated to the iMTN below the YCL and surrounding the lipid granules (see Supplement 1 Fig. S3). The use of non-fixed samples, the enhanced quantum efficiency of the sCMOS sensors and the extended penetration depth provided by the LSFM technique give us the power to detect the weak signal coming from the iMTN, normally hidden in previous studies. Therefore, this work adds a new MTs set to the zebrafish embryonic model.

This newly found network inside the yolk is present during the whole early embryonic development: we visualized it in non-fertilized eggs, and at cleavage (Supplementary Fig. S4), blastula, and epiboly (Fig. 7(A), Visualization 6) stages. In studying the dynamics of this MT network, we investigated how its links to the eMTN are affected from a MOW travelling in the YCL. We found that at the MOW passage, connections between the iMTN and the eMTN are lost and that new connections are formed afterwards (Fig. 7(B)-(D), Visualization 7, and Supplementary Fig. S4). A similar dynamics was also found at the connection between the iMTN and the eYSN during the nuclei divisions: the link is temporarily lost at mitosis, and re-established shortly after with the nuclei resulting from the division (Fig. 7(E)-(G), Visualization 4 and Visualization 5).

The evidences found on the morphology and dynamic characteristics of this iMTN, and its connection with the MOW phenomena, provide therefore a novel view on the description of the MT networks populating the yolk cell in the zebrafish's early embryonic development, as depicted in Fig. 7(H).

Biomedical Optics EXPRESS

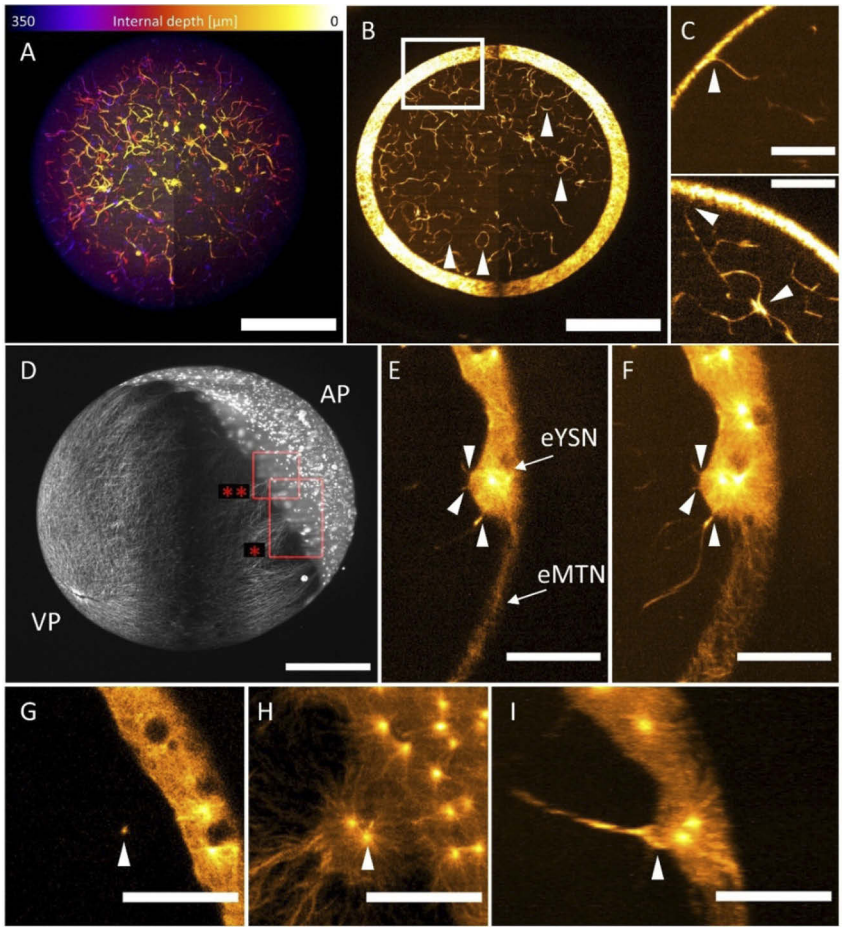

Fig. 6. Internal MT network morphology. (A) Depth-coded projection of a z-stack in which the information relative to the outer YCL was digitally removed. The internal microtubule network and its extension within the yolk is visible. Visualized depths range between 0 µm (white) and 350 µm (blue). Vegetal view, left and right images of the embryo are stitched together, scale bar 200 µm. (B) Maximum intensity projection over a 40 µm range of a yolk section. The internal MTs forms circular patterns (white arrows) and also are connected to the external yolk MTs (eMTN) network. Vegetal view, left and right images of the embryo are stitched together, scale bar 200 µm. (C) Zoom (single slices) on the yolk surface, showing clear connections between the internal and external MT networks (white arrows, upper and lower panel), and interconnections between internal MTs (white arrow, lower panel). Scale bars 50 µm. (D) Embryo at sphere stage, lateral view. AP = animal pole, VP = vegetal pole, scale bar 200 µm. (E) zoom into the ROI indicated by * in (D), single slice, showing connection of internal MTs to an eYSN (white arrows). eMTN = external MT network, scale bar 50 µm. (F) Maximum intensity projection over a 20 µm range of the same ROI showing also the extension toward the internal portion of the yolk of the MT connected to an eYSN. Scale bar 50 µm. See also Visualization 5. (G) zoom into the ROI indicated by ** in (D), single slice, showing an internal MT bundle (white arrow) extending perpendicular to the image plane. (H) Maximum intensity projection showing the end point of that internal MT bundle, coinciding with a centriole (white arrow) associated to an eYSN. (I) An XZ re-slice view of the same ROI showing the connection of the same MT bundle and its extension toward the interior of the yolk. Scale bars 50 µm. See also Visualization 4. All figures relative to dclk2-GFP embryos, and Orange HOT lookup table was used to ease iMTN visualization.

Biomedical Optics EXPRESS

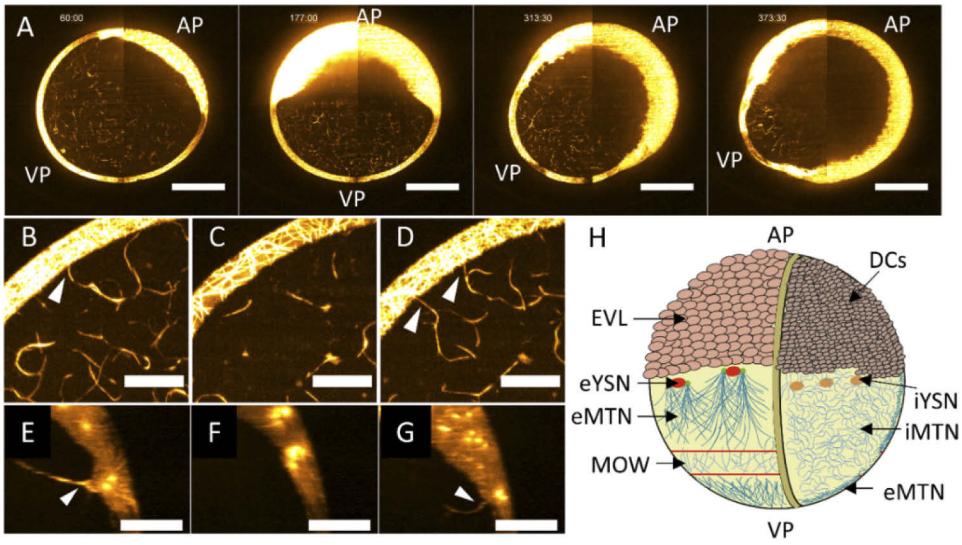

Fig. 7. Internal MT network dynamics. (A) Time series visualizing a maximum intensity projection over a 30 µm of a developing embryo from (left to right) blastula, 50%, 70%, and 90% epiboly. The iMTN is visible in all these stages. AP = animal pole, VP = vegetal pole. Left and right images of the embryo are stitched together, scale bars 200 µm. See also Visualization 6. (B-D) Time series visualizing through maximum intensity projection over 26 µm the dynamics of iMTN-eMTN connections upon MOW passage. Before MOW passage the connection is clearly visible (white arrow, B), during MOW passage the connection is lost (C), and is re-established after MOW passage (white arrows, D). Scale bars 50 µm. See also Visualization 7. Single slice images relative to the same frame of (B) and (D) are visible in Supplementary Fig. S4. (E-G) Time series visualizing the XZ re-slice dynamics of iMTN-eYSN connection upon eYSN mitosis. Before the eYSN division the connection is present (E), during the division the connection is lost (F), and re-established after the division is completed (G). Scale bars 50 µm. All figures relative to dclk2-GFP embryos, and Orange HOT lookup table was used to ease iMTN visualization. (H) Updated model for the MT networks populating the zebrafish yolk between 512-cell and sphere stages. On the left side, the eMTN associated to the eYSN is subject to the MOW travelling toward the VP, exemplified as a belt of low-density MT. On the right side, the section view of the embryo is illustrated. The iMTN is present within the whole yolk cell. EVL = enveloping layer, DCs = deep cells. Representation not in scale.

Biomedical Optics EXPRESS

4. Discussion

Previous works have shown the presence of two sets of MTs network in the zebrafish yolk cell: (1) a MTs mesh surrounding the iYSN and (2) a vegetally oriented MTs array in the YCL [6–8]. The latter MTs array, here called eMTN, is associated with the marginal blastomeres and subsequently to the eYSN [7], and it has been particularly studied during the epibolic process due to its important connection with the eYSN migration [9]. However, prior to the epiboly stage, the network has been mainly investigated either on fixed samples [3,7] or through restricted field of views [10,11,34], or in limited time windows [10]. In this work we developed experimental setups and workflows to effectively visualize and analyze the yolk MTs structures. With this we can contribute to fill the current lack of *in vivo* studies on the MTs arrays during cleavage, blastula and epiboly stages and reveal important morphologies and dynamics which were, to our knowledge, until now hidden. LSFM emerges as the ideal tool for this particular application providing unprecedented penetration depth, high signal to noise ratios, large FoVs, and limited photobleaching [21]. These capabilities permit the study of MTs in the whole embryo for extended time windows. The correct development of the sample is also ensured by the possibility of controlling the temperature of the imaging environment and the absence of sample mounting medium's mechanical constrictions, as the zebrafish develops inside its own chorion.

Our results show that the MT networks filling the zebrafish yolk in the early embryonic development present more complex characteristics than previously thought. Through this work we provide an important update on the current view [3,6–8] on the yolk's MT populations, schematically represented in Fig. 7(H). The eMTN, located at the YCL, is associated with marginal blastomeres or, as the YSL forms, with the eYSN. Corresponding to each mitotic wave that involves the MT branch-associated nuclei, a MOW is initiated and travels over the YCL from the blastoderm margin to the vegetal pole, and it re-organizes the eMTN in thicker and sparser bundles. MOWs appear to travel in a belt-like fashion concentrically closing at the vegetal pole. Moreover, an intricated iMTN is present in the whole inner part of the yolk, and it presents clear connections with the eMTN. These links are lost upon the passage of a MOW and new connections are re-established shortly after. In addition, the iMTN also appear connected to eYSN. This means that eYSN are associated not only with the AV parallel MTs array, as already known, but also to the iMTN. Upon eYSN mitosis, the connection is lost and re-established shortly after as well. Therefore, we found that the view describing a microtubule mesh in the iYSL [6–8] is partial in both space and time. Thanks to the intrinsic capabilities of LSFM, we in fact demonstrate that a MT mesh extends in the whole inner yolk, and that it is present not only when the YSL forms, but in the whole embryonic development from non-fertilized eggs until at least the end of epiboly.

The MOWs described here may correspond to what Chen et al. observed and defined as a "microtubule turnover" [11]. Nevertheless, the description provided in their work of the phenomena has been done in a limited region of the MT network, in restricted time windows and focused on the examination of Dachsous1b interactions with Aurora B and Ttc28 proteins [11], providing a complementary molecular study on YCL MTs. Our efforts go towards the mesoscopic description of the MOW phenomena, revealing the dynamics of the entire eMTN and defining this wave-like pattern over extended time windows. We provide evidences demonstrating a strong dependence between the mitotic cycles of the blastoderm (and when formed, of the YSN) with the MOWs' initiations. We hypothesize that MOWs are necessary to re-organize the eMTN after each blastomere/eYSN division to connect the extremely long MTs branches to the newly generated centrosomes, and thus to allow the following epibolic eYSN migration along the so organized network.

With the combination of large FoVs and extended time windows, our global analysis permits to visualize the mitotic waves [1,16,17] in the blastoderm, and how the MOWs, after being initiated, propagate towards the vegetal pole. This dedicated image-analysis tool enables as

Biomedical Optics EXPRESS

well the evaluation of their speed along the meridians of the yolk sphere. The MOWs' velocity values calculated in this work, although depending on the developmental temperature and on the current developmental stage, fit within the order of magnitude of the propagation speeds of other wave-patterns already observed in zebrafish embryos, such as bulk actin polymerization waves (ranging from approx. 20 to 70 µm/min [13]) and mitotic waves (ranging from approx. 10 to 65 µm/min [16,17]). Thus, this analysis allows to have an automatic tool for a global view of the wave-like processes until the end of blastula stages, considering the entire embryo dynamics and shape. We consider this analysis of particular interest for the application on the yolk's MTs, as described in this work, and also in MT mutant phenotypes [2], that would permit a global approach to their study during extended time windows. Moreover, it could help the examination also of other spherical-based dynamics in zebrafish such as the mitotic waves [1,16,17] and calcium waves [14,35], both in mutant embryos and in their wild-type counterparts. In addition, the same tool can be used also in investigating other spherical organisms (e.g. Xenopus embryos). Besides that, the analysis along the parallels provides a way to understand eventual bias of the wave patterns with respect to the dorsal-ventral axis.

Although the nature of the MOW wave-like pattern remains unclear, due to the large size of the yolk and the relative fast propagation of the MOWs, the chemical wave model could be a possible explanation. In [19] the authors demonstrated that a Cdk1 activation wave is responsible for the visualized nuclear envelopes' dynamics synchronization *in vitro*. Such a wave is an example of "chemical wave" [12,26] (also called "trigger wave" [36]), and accounts for the propagation of the event in consideration through its subsequent activations on the neighboring areas, allowing the signal to advance. A link to support that MOWs are indeed chemical waves can be found in [26], in which is proposed that a chemical wave could account for large MT aster's growth, and that the centrosome could act as wave initiation site. Moreover, Ishihara et al. speculate about possible cross talks between mitotic and microtubule chemical waves for large cells organization [26]. The yolk MTs emanated from blastomeres and eYSN centrosomes of the zebrafish embryo could be a model to study these hypotheses *in vivo*, using the tools proposed in this work. Further studies are needed to understand how such intricated and large MT networks (both the eMTN and the iMTN) are nucleated and capable to extend in a large volume like the yolk cell. Ishihara et al. propose that MT nucleation can be stimulated far away from centrosomes by pre-existing MTs [26]. This hypothesis would explain the fact that MTs belonging to large asters do not appear to decrease in density with the increase of the distance from the centrosome, which would be expected if all MTs minus end were connected to it. The large microtubules branches of the zebrafish eMTN, together with its dynamics here described, and the connections to the iMTN found in this work could be a model to test this hypothesis *in vivo*, also considering recent findings on non-centrosomal MT organizing centers [9,27].

We believe that the observation of the cyclic MOW process and the visualization of the iMTN have a critical importance in the complete description of the microtubule networks of the yolk. It shows the necessity to visualize and analyze the microtubule networks in live samples and with a relatively large FoV, both characteristics enabled by LSFM. Therefore, we consider that the characterization of the networks' organization cannot be solely performed in a "static" way, but it must also be described in its dynamic dimension. In fact, the analysis of the microtubules in fixed samples could bring misleading conclusions about their actual arrangement as in the moment of the fixation is probably not known if the MOW has already given its effect or not, but more importantly because we showed that the network is not a static organization. Concluding, our study permits providing a novel insight on yolk's MT morphology and dynamics, and offers a basis to LSFM methodologies for studying new and already approached aspects of the yolk MT networks.

Funding. Horizon 2020 Framework Programme (Marie Sklodowska-Curie 721537); Laserlab-Europe (871124);

Biomedical Optics EXPRESS

Ministerio de Economía y Competitividad (RYC-2015-17935); Generalitat de Catalunya (CERCA Program); Fundación Cellex (Fundación Mir-Puig); Ministerio de Economía y Competitividad (CEX2019-000910-S).

Acknowledgments. MB, MM, and EJG designed the experiments. MB and EJG built the microscopes and conducted the experiments. MB conducted the data and statistical analysis, and wrote the manuscript. All authors reviewed and edited the manuscript. MB, EJG, MM and PLA conceptualized the study. PLA supervised the work.

Disclosures. The authors declare no conflict of interests.

Data availability. Data underlying the results presented in this paper are not publicly available at this time but may be obtained from the authors upon reasonable request.

Supplemental document. See Supplement 1 for supporting content.

References

1. C. B. Kimmel, W. W. Ballard, S. R. Kimmel, B. Ullmann, and T. F. Schilling, "Stages of embryonic development of the zebrafish," Dev. Dyn. **203**(3), 253–310 (1995).
2. N. Li-Villarreal, M. M. Forbes, A. J. Loza, J. Chen, T. Ma, K. Helde, C. B. Moens, J. Shin, A. Sawada, A. E. Hindes, J. Dubrulle, A. F. Schier, G. D. Longmore, F. L. Marlow, and L. Solnica-Krezel, "Dachsous1b cadherin regulates actin and microtubule cytoskeleton during early zebrafish embryogenesis," Development **142**(15), 2704–2718 (2015).
3. S. Jesuthasan and U. Stähle, "Dynamic microtubules and specification of the zebrafish embryonic axis," Curr. Biol. **7**(1), 31–42 (1997).
4. A. V Gore and K. Sampath, "Localization of transcripts of the zebrafish morphogen Squint is dependent on egg activation and the microtubule cytoskeleton," Mech. Dev. **112**(1-2), 153–156 (2002).
5. R. Fuentes and J. Fernández, "Ooplasmic segregation in the zebrafish zygote and early embryo: pattern of ooplasmic movements and transport pathways," Dev. Dyn. **239**(8), 2172–2189 (2010).
6. A. E. E. Bruce, "Zebrafish epiboly: Spreading thin over the yolk," Dev. Dyn. **245**(3), 244–258 (2016).
7. L. Solnica-Krezel and W. Driever, "Microtubule arrays of the zebrafish yolk cell: organization and function during epiboly," Development **120**(9), 2443–2455 (1994).
8. S. E. Lepage and A. E. E. Bruce, "Zebrafish epiboly: mechanics and mechanisms," Int. J. Dev. Biol. **54**(8-9), 1213–1228 (2010).
9. Z. Fei, K. Bae, S. E. Parent, H. Wan, K. Goodwin, U. Theisen, G. Tanentzapf, and A. E. E. Bruce, "A cargo model of yolk syncytial nuclear migration during zebrafish epiboly," Development **146**(1), dev169664 (2019).
10. L. D. Tran, H. Hino, H. Quach, S. Lim, A. Shindo, Y. Mimori-Kiyosue, M. Mione, N. Ueno, C. Winkler, M. Hibi, and K. Sampath, "Dynamic microtubules at the vegetal cortex predict the embryonic axis in zebrafish," Development **139**(19), 3644–3652 (2012).
11. J. Chen, G. D. Castelvecchi, N. Li-Villarreal, B. Raught, A. M. Krezel, H. McNeill, and L. Solnica-Krezel, "Atypical Cadherin Dachsous1b Interacts with Ttc28 and Aurora B to control microtubule dynamics in embryonic cleavages," Dev. Cell **45**(3), 376–391.e5 (2018).
12. V. E. Deneke and S. Di Talia, "Chemical waves in cell and developmental biology," J. Cell Biol. **217**(4), 1193–1204 (2018).
13. S. Shamipour, R. Kardos, S.-L. Xue, B. Hof, E. Hannezo, and C.-P. Heisenberg, "Bulk actin dynamics drive phase segregation in zebrafish oocytes," Cell 177(6), 1463–1479.e18 (2019).
14. S. E. Webb and A. L. Miller, "Ca^{2+} signaling and early embryonic patterning during the blastula and gastrula periods of zebrafish and Xenopus development," Biochim. Biophys. Acta **1763**(11), 1192–1208 (2006).
15. E. Gilland, A. L. Miller, E. Karplus, R. Baker, and S. E. Webb, "Imaging of multicellular large-scale rhythmic calcium waves during zebrafish gastrulation," Proc. Natl. Acad. Sci. U. S. A. **96**(1), 157–161 (1999).
16. P. J. Keller, A. D. Schmidt, J. Wittbrodt, and E. H. K. Stelzer, "Reconstruction of zebrafish early embryonic development by scanned light sheet microscopy," Science **322**(5904), 1065–1069 (2008).
17. N. Olivier, M. A. Luengo-Oroz, L. Duloquin, E. Faure, T. Savy, I. Veilleux, X. Solinas, D. Débarre, P. Bourgine, A. Santos, N. Peyriéras, and E. Beaurepaire, "Cell lineage reconstruction of early zebrafish embryos using label-free nonlinear microscopy," Science **329**(5994), 967–971 (2010).
18. G. A. Anderson, L. Gelens, J. C. Baker, and J. E. J. Ferrell, "Desynchronizing embryonic cell division waves reveals the robustness of xenopus laevis development," Cell Rep. **21**(1), 37–46 (2017).
19. J. B. Chang and J. E. J. Ferrell, "Mitotic trigger waves and the spatial coordination of the Xenopus cell cycle," Nature **500**(7464), 603–607 (2013).
20. J. Huisken, J. Swoger, F. Del Bene, J. Wittbrodt, and E. H. K. Stelzer, "Optical sectioning deep inside live embryos by selective plane illumination microscopy," Science **305**(5686), 1007–1009 (2004).
21. O. E. Olarte, J. Andilla, E. J. Gualda, and P. Loza-Alvarez, "Light-sheet microscopy: a tutorial," Adv. Opt. Photonics **10**(1), 111–179 (2018).
22. J. Huisken and D. Y. R. Stainier, "Selective plane illumination microscopy techniques in developmental biology," Development **136**(12), 1963–1975 (2009).
23. B. Schmid, G. Shah, N. Scherf, M. Weber, K. Thierbach, C. P. Campos, I. Roeder, P. Aanstad, and J. Huisken, "High-speed panoramic light-sheet microscopy reveals global endodermal cell dynamics," Nat. Commun. **4**(1), 2207 (2013).

Biomedical Optics EXPRESS

24. G. Shah, K. Thierbach, B. Schmid, J. Waschke, A. Reade, M. Hlawitschka, I. Roeder, N. Scherf, and J. Huisken, "Multi-scale imaging and analysis identify pan-embryo cell dynamics of germlayer formation in zebrafish," Nat. Commun. **10**(1), 5753 (2019).
25. E. J. Gualda, H. Pereira, T. Vale, M. F. Estrada, C. Brito, and N. Moreno, "SPIM-fluid: open source light-sheet based platform for high-throughput imaging," Biomed. Opt. Express **6**(11), 4447–4456 (2015).
26. K. Ishihara, P. A. Nguyen, M. Wühr, A. C. Groen, C. M. Field, and T. J. Mitchison, "Organization of early frog embryos by chemical waves emanating from centrosomes," Phil. Trans. R. Soc. B **369**(1650), 20130454 (2014).
27. M. Marsal, M. Bernardello, E. J. Gualda, and P. Loza-Alvarez, "The microtubule organization in the zebrafish yolk adapts to transgene-mediated phenotypic variations," bioRxiv 2020.08.06.239970 (2020), https://www.biorxiv.org/content/10.1101/2020.08.06.239970v2.
28. J. Schindelin, I. Arganda-Carreras, E. Frise, V. Kaynig, M. Longair, T. Pietzsch, S. Preibisch, C. Rueden, S. Saalfeld, B. Schmid, J.-Y. Tinevez, D. J. White, V. Hartenstein, K. Eliceiri, P. Tomancak, and A. Cardona, "Fiji: an open-source platform for biological-image analysis," Nat. Methods **9**(7), 676–682 (2012).
29. S. Preibisch, S. Saalfeld, and P. Tomancak, "Globally optimal stitching of tiled 3D microscopic image acquisitions," Bioinformatics **25**(11), 1463–1465 (2009).
30. J.-Y. Tinevez, N. Perry, J. Schindelin, G. M. Hoopes, G. D. Reynolds, E. Laplantine, S. Y. Bednarek, S. L. Shorte, and K. W. Eliceiri, "TrackMate: an open and extensible platform for single-particle tracking," Methods **115**, 80–90 (2017).
31. L. Carvalho and C.-P. Heisenberg, "The yolk syncytial layer in early zebrafish development," Trends Cell Biol. **20**(10), 586–592 (2010).
32. Š. Bálint, I. Verdeny Vilanova, Á. Sandoval Álvarez, and M. Lakadamyali, "Correlative live-cell and superresolution microscopy reveals cargo transport dynamics at microtubule intersections," Proc. Natl. Acad. Sci. U. S. A. **110**(9), 3375–3380 (2013).
33. J. Topczewski and L. Solnica-Krezel, "Cytoskeletal dynamics of the zebrafish embryo," Methods Cell Biol. **59**, 205–226 (1998).
34. L. Fontenille, S. Rouquier, G. Lutfalla, and D. Giorgi, "Microtubule-associated protein 9 (Map9/Asap) is required for the early steps of zebrafish development," Cell Cycle **13**(7), 1101–1114 (2014).
35. S. E. Webb and A. L. Miller, "Calcium signalling during zebrafish embryonic development," Bioessays **22**(2), 113–123 (2000).
36. L. Gelens, G. A. Anderson, and J. E. J. Ferrell, "Spatial trigger waves: positive feedback gets you a long way," Mol. Biol. Cell **25**(22), 3486–3493 (2014).